Author(s): Garaud, Julien; Corticelli, Alberto; Silaev, Mikhail; Babaev, Egor

Title: Field-induced coexistence of s++ and s± superconducting states in dirty multiband superconductors

Year: 2018

Version:

Please cite the original version:

Garaud, J., Corticelli, A., Silaev, M., & Babaev, E. (2018). Field-induced coexistence of s++ and s± superconducting states in dirty multiband superconductors. Physical Review B, 97(5), 054520. https://doi.org/10.1103/PhysRevB.97.054520

Field-induced coexistence of s_{++} and $s_{\pm}$ superconducting states in dirty multiband superconductors

Julien Garaud,[1,2] Alberto Corticelli,[1] Mihail Silaev,[3] and Egor Babaev[1]
[1]*Department of Physics, KTH-Royal Institute of Technology, Stockholm SE-10691, Sweden*
[2]*Laboratoire de Mathématiques et Physique Théorique CNRS/UMR 7350, Fédération Denis Poisson FR2964, Université de Tours, Parc de Grandmont, 37200 Tours, France*
[3]*Department of Physics and Nanoscience Center, University of Jyväskylä, P.O. Box 35 (YFL), FI-40014 University of Jyväskylä, Finland*

(Received 26 December 2017; revised manuscript received 15 February 2018; published 28 February 2018)

In multiband systems, such as iron-based superconductors, the superconducting states with locking and antilocking of the interband phase differences are usually considered as mutually exclusive. For example, a dirty two-band system with interband impurity scattering undergoes a sharp crossover between the $s_{\pm}$ state (which favors phase antilocking) and the s_{++} state (which favors phase locking). We discuss here that the situation can be much more complex in the presence of an external field or superconducting currents. In an external applied magnetic field, dirty two-band superconductors do not feature a sharp $s_{\pm} \to s_{++}$ crossover but rather a washed-out crossover to a finite region in the parameter space where both $s_{\pm}$ and s_{++} states can coexist for example as a lattice or a microemulsion of inclusions of different states. The current-carrying regions such as the regions near vortex cores can exhibit an $s_{\pm}$ state while it is the s_{++} state that is favored in the bulk. This coexistence of both states can even be realized in the Meissner state at the domain's boundaries featuring Meissner currents. We demonstrate that there is a magnetic-field-driven crossover between the pure $s_{\pm}$ and the s_{++} states.

DOI: 10.1103/PhysRevB.97.054520

I. INTRODUCTION

It is widely accepted that in iron-based superconductors, the pairing between electrons is produced by interband electron-electron repulsion [1–3]. In such a situation, the superconducting state, which features a sign inversion between the two s-wave gap functions, is called $s_{\pm}$, in contrast to the s_{++} state, which has no sign inversion. The presence of disorder is known to potentially lead to a crossover from the $s_{\pm}$ to the s_{++} state [4]. In the absence of an external magnetic field, the crossover is sharp and has basically no thermodynamic features. It was however recently demonstrated that the crossover line is accompanied by a nontrivial transition in the core structure of vortices [5]. More precisely the vortices, in the vicinity of the crossover line, can acquire a circular nodal line around the singular point in one of the superconducting components [5]. This singular nodal line, which in three dimensions extends to a cylindrical nodal surface surrounding the vortex line, results in the formation of a peculiar "moat"-like profile in the subdominant component of the superconducting gap. As a result, the inner region of the vortex core shows a π relative phase between the gaps while it is zero in the outer region. This means that these moat-core vortices consist of an $s_{\pm}$ phase inclusion in the vortex core, which is separated from the bulk s_{++} phase by the nodal line. Here we investigate the consequences of that physics on the phase diagram of such dirty two-band superconductors, in an external magnetic field. In a low applied external field the lattices and liquids of such moat-core vortices represent a phase coexistence or a mircoemulsion of such $s_{\pm}$ inclusions inside the bulk s_{++} state. At elevated fields this results in a field-induced transition between the $s_{\pm}$ and s_{++} states.

We start our investigation, in Sec. II, by deriving a two-band Ginzburg-Landau model (including the gradient terms) from the microscopic Usadel theory of dirty two-band superconductors and discuss the essential properties of the phase diagram. Next, Sec. III is devoted to the investigation of the physical properties of the elementary topological excitations (the vortices) and their core structure in that model. There, we show that across the $s_{\pm}/s_{++}$ crossover line there is a structural transition in the core of topological excitations, and we further construct the diagram where such solutions occur, as a function of the system's microscopic parameters. In Sec. IV we investigate the consequences for the phase diagram in an applied external magnetic field, and finally our conclusions are presented in Sec. V.

II. THEORETICAL FRAMEWORK

Within a weak-coupling approximation, two-band superconductors with a high concentration of impurities can be described by a system of two Usadel equations, coupled by interband impurity-scattering terms (see, e.g., [6]):

$$\omega_n f_i = \frac{D_i}{2}(g_i \mathbf{\Pi}^2 f_i - f_i \nabla^2 g_i) + \Delta_i g_i + \sum_{j \neq i} \gamma_{ij}(g_i f_j - g_j f_i). \quad (1)$$

Here $\omega_n = (2n+1)\pi T$ (with $n \in \mathbb{Z}$) are the Matsubara frequencies. T is the temperature, D_i are the electron diffusivities, and γ_{ij} are the interband scattering rates. The quasiclassical propagators f_i and g_i are respectively the anomalous and normal Green's functions in each band, which obey the normalization condition $|f_i|^2 + g_i^2 = 1$. The components of the order parameter $\Delta_j = |\Delta_j| e^{i\theta_j}$ are determined by the

self-consistency equations

$$\Delta_i = 2\pi T \sum_{n=0}^{N_d} \sum_j \lambda_{ij} f_j(\omega_n), \tag{2}$$

for the Green's functions that satisfy Eq. (1). Here, $N_d = \Omega_d/(2\pi T)$ is the summation cutoff at Debye frequency Ω_d. The diagonal elements λ_{ii} of the coupling matrix $\hat{\lambda}$ in the self-consistency equation (2) describe the intraband pairing, while the interband interaction is determined by the off-diagonal terms λ_{ij} $(j \neq i)$. The interband coupling parameters and impurity scattering amplitudes satisfy the symmetry relation [6]

$$\lambda_{ij} = -\lambda_J/N_i \text{ with } j \neq i, \text{ and } \gamma_{ij} = \Gamma N_j, \tag{3}$$

where $\lambda_J, \Gamma > 0$, and $N_{1,2}$ are the partial densities of states in the two bands.

In order to investigate the physical properties of dirty two-band superconductors in the external field, we consider a Ginzburg-Landau (GL) model that is derived from the microscopic Usadel theory of dirty superconductors. The Ginzburg-Landau free energy functional for multiband models is obtained as an expansion in several small parameters: small gaps and gradients (not to be confused with a symmetry-based GL expansion that uses a single small parameter τ; see also remark [7]). The resulting expression, including gradient terms, reads as [5]

$$\frac{\mathcal{F}}{\mathcal{F}_0} = \sum_{j=1}^{2} \left(\frac{k_{jj}}{2} |\mathbf{\Pi}\Delta_j|^2 + a_{jj}|\Delta_j|^2 + \frac{b_{jj}}{2}|\Delta_j|^4 \right) \tag{4a}$$

$$+ \frac{k_{12}}{2}[(\mathbf{\Pi}\Delta_1)^* \mathbf{\Pi}\Delta_2 + (\mathbf{\Pi}\Delta_2)^* \mathbf{\Pi}\Delta_1] \tag{4b}$$

$$+ 2(a_{12} + c_{11}|\Delta_1|^2 + c_{22}|\Delta_2|^2)\mathrm{Re}(\Delta_1^*\Delta_2) \tag{4c}$$

$$+ (b_{12} + c_{12}\cos 2\theta_{12})|\Delta_1|^2|\Delta_2|^2 + \frac{\boldsymbol{B}^2}{2}. \tag{4d}$$

Here, the complex fields $\Delta_j = |\Delta_j| e^{i\theta_j}$ represent the superconducting gaps in the different bands, and $\theta_{12} = \theta_2 - \theta_1$ stands for the relative phase between them. The two gaps in the different bands are electromagnetically coupled by the vector potential $\boldsymbol{A}$ of the magnetic field $\boldsymbol{B} = \nabla \times \boldsymbol{A}$, through the gauge derivative $\mathbf{\Pi} \equiv \nabla + iq\boldsymbol{A}$, and the coupling constant q parametrizes the penetration depth of the magnetic field.

The coefficients of the Ginzburg-Landau functional a_{ij}, b_{ij}, c_{ij}, and k_{ij} are calculated from a given set of input parameters λ_{ij}, D_i, T, and Γ of the microscopic self-consistent equation. First, the coefficients of gradient terms are given by [5]

$$k_{ii} = 2\pi T N_i \sum_{n=0}^{N_d} \frac{D_i(\omega_n + \gamma_{ji})^2 + \gamma_{ij}\gamma_{ji} D_j}{\omega_n^2(\omega_n + \gamma_{ij} + \gamma_{ji})^2}, \tag{5a}$$

$$k_{ij} = 2\pi T N_i \gamma_{ij} \sum_{n=0}^{N_d} \frac{D_i(\omega_n + \gamma_{ji}) + D_j(\omega_n + \gamma_{ij})}{\omega_n^2(\omega_n + \gamma_{ij} + \gamma_{ji})^2}, \tag{5b}$$

with $j \neq i$. Next, the coefficients of the potential terms are

$$a_{ii} = \frac{N_i \lambda_{jj}}{\det(\hat{\lambda})} - 2\pi T \sum_{n=0}^{N_d} \frac{(\omega_n + \gamma_{ji})N_i}{\omega_n(\omega_n + \gamma_{ij} + \gamma_{ji})}, \tag{6a}$$

$$a_{ij} = -\frac{N_i \lambda_{ij}}{\det(\hat{\lambda})} - 2\pi T \sum_{n=0}^{N_d} \frac{\gamma_{ij} N_i}{\omega_n(\omega_n + \gamma_{ij} + \gamma_{ji})}. \tag{6b}$$

The other parameters read as

$$b_{ii} = \pi T N_i \sum_{n=0}^{N_d} \frac{(\omega_n + \gamma_{ji})^4}{\omega_n^3(\omega_n + \gamma_{ij} + \gamma_{ji})^4}$$

$$+ \pi T N_i \sum_{n=0}^{N_d} \frac{\gamma_{ij}(\omega_n + \gamma_{ji})\left(\omega_n^2 + 3\omega_n\gamma_{ji} + \gamma_{ji}^2\right)}{\omega_n^3(\omega_n + \gamma_{ij} + \gamma_{ji})^4}, \tag{7a}$$

$$b_{ij} = -\pi T N_i \sum_{n=0}^{N_d} \frac{\gamma_{ij}}{(\omega_n + \gamma_{ij} + \gamma_{ji})^4} + \pi T N_i$$

$$\times \sum_{n=0}^{N_d} \frac{\gamma_{ij}(\gamma_{ij} + \gamma_{ji})[\omega_n(\gamma_{ij} + \gamma_{ji}) + 2\gamma_{ij}\gamma_{ji}]}{\omega_n^3(\omega_n + \gamma_{ij} + \gamma_{ji})^4}, \tag{7b}$$

and

$$c_{ii} = \pi T N_i \sum_{n=0}^{N_d} \frac{\gamma_{ij}(\omega_n + \gamma_{ji})\left[\omega_n^2 + (\omega_n + \gamma_{ji})(\gamma_{ij} + \gamma_{ji})\right]}{\omega_n^3(\omega_n + \gamma_{ij} + \gamma_{ji})^4}, \tag{8a}$$

$$c_{ij} = \pi T N_i \sum_{n=0}^{N_d} \frac{\gamma_{ij}(\omega_n + \gamma_{ji})(\omega_n + \gamma_{ij})(\gamma_{ij} + \gamma_{ji})}{\omega_n^3(\omega_n + \gamma_{ij} + \gamma_{ji})^4}. \tag{8b}$$

In Eq. (5), the coefficients of the gradient terms depend on electronic diffusivity coefficients D_1 and D_2. The parameter space can be reduced by absorbing one of the electronic diffusivity coefficients in the gradient term. Without loss of generality, we choose D_1 to be the largest diffusivity coefficient $(D_1 > D_2)$. Thus, in the dimensionless units, the coefficients of the gradient term depend only on the ratio of diffusivities, or *diffusivity imbalance* $r_d = D_2/D_1 < 1$. We define the dimensionless variables by normalizing the gaps by T_c and the lengths by $\xi_0 = \sqrt{D_1/T_c}$. The magnetic field by is scaled $B_0 = T_c\sqrt{4\pi N_1}$, where N_1 is the density of states in the first band, and the free energy $\mathcal{F}_0 = B_0^2/4\pi$. The electromagnetic coupling constant is $q = 2\pi B_0 \xi_0^2/\Phi_0$. In these units, the London penetration length λ_L is given by $\lambda_L^{-2} = q^2(k_{ii}\Delta_{i0}^2 + 2k_{12}\Delta_{10}\Delta_{20})$, where Δ_{i0} is the bulk value of the dimensionless gap.

It was demonstrated in Ref. [9] that, within its range of applicability, the two-band Ginzburg-Landau formalism (4) indeed produces phase diagrams that match those of the microscopic theory even at temperatures substantially lower than the critical temperature T_c of the superconducting phase transition. Figure 1 shows such a phase diagram in the case of a two-band superconductor with nearly degenerate bands ($\lambda_{11} = 0.29$ and $\lambda_{22} = 0.3$), and intermediate repulsive interband pairing interaction ($\lambda_{12} = \lambda_{21} = -0.05$). The regions of different ground state relative phases clearly identify the different phases. This illustrates that the presence of disorder leads to a crossover from the $s_\pm$ to the s_{++} state. In the absence of an external magnetic field, the crossover is sharp as can be seen by the solid black line that shows the crossover between $s_\pm$ and s_{++} states, where the subdominant gap Δ_1 vanishes.

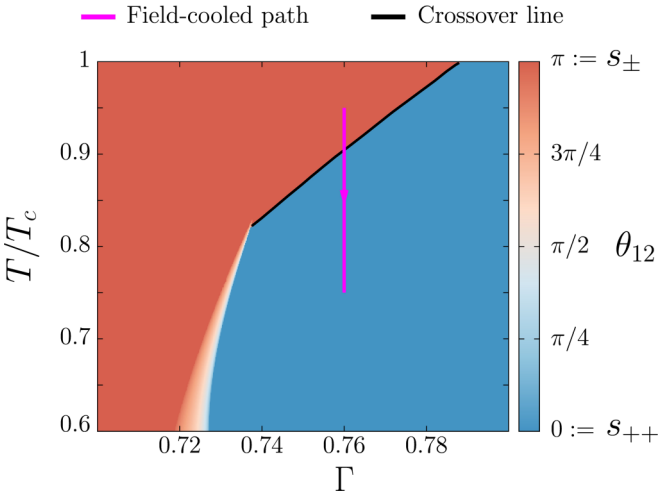

FIG. 1. Example of a phase diagram of the Ginzburg-Landau free energy describing two-band superconductors with interband impurity scattering. It shows the values of the lowest-energy state relative phase $\theta_{12} = \theta_2 - \theta_1$ between the two components of the order parameter, as a function of temperature and interband scattering amplitude Γ. The coupling matrix $\hat{\lambda}$ corresponds to $\lambda_{11} = 0.29$ and $\lambda_{22} = 0.3$ with intermediate $\lambda_{12} = \lambda_{21} = -0.05$ repulsive interband pairing interaction. The solid black line shows the zero of the subdominant gap Δ_1, which is the crossover between $s_{\pm}$ and s_{++} states. The vertical line shows a field-cooling path realized later for a simulation in the external field.

Another interesting transition between the s_{++} and the $s_{\pm}$ phases is possible. Indeed, as a results of the presence of impurities, a possibility for an additional phase appears. This extra phase, where the interband phase difference $\theta_{12} = \theta_2 - \theta_1$ is neither zero nor π, is termed the $s + is$ state. The fact that the interband phase difference can be such that $\theta_{12} \neq 0, \pi$ follows from the existence of phase-locking terms $\propto \cos\theta$ in (4c) and the others that are $\propto \cos 2\theta$ in (4c). The competition between those terms is responsible for the existence of the impurity-induced $s + is$ state [10]. The s-wave states that spontaneously break the time-reversal symmetry have been a subject of much interest in recent years; see, e.g., [9–17]. In this work, we focus on the physics of the direct $s_{\pm}$ to the s_{++} impurity-induced crossover in an external magnetic field (denoted by the solid black line on Fig. 1). Although the physics of vortices in, and in the vicinity of, the $s + is$ is very rich, it is beyond the scope of the current work and its detailed study will be addressed in a subsequent work [18].

Below, we discuss that in an external applied magnetic field, dirty two-band superconductors do not feature a sharp $s_{\pm} \to s_{++}$ crossover but there appears a finite region in the parameter space where both $s_{\pm}$ and s_{++} states can coexist in a peculiar way.

III. STRUCTURAL TRANSITION OF VORTEX CORES

When going from the s_{++} to $s_{\pm}$ state, there is a transition in the vortex core structure: the vortices there can develop an additional circular nodal line around the singular point in one of the superconducting components [5]. Thus these vortices consist of an $s_{\pm}$ phase inclusion in the vortex core, which is separated from the bulk s_{++} phase by the nodal line.

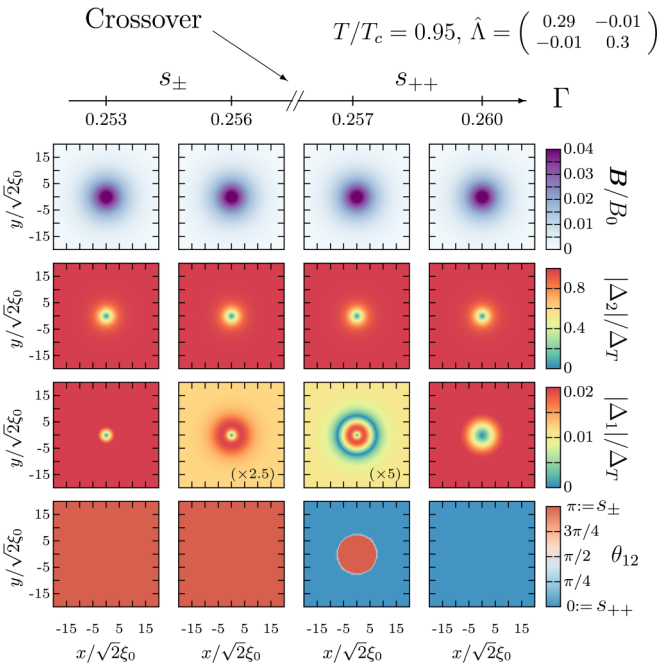

FIG. 2. Vortex configurations in the vicinity of the impurity induced crossover line of a two-band superconductor. The temperature here is $T/T_c = 0.95$, $q = 0.5$, and tuning the strength of the interband impurity scattering drives the ground state from bulk s_{++} to bulk $s_{\pm}$. The different lines respectively display the magnetic field $\boldsymbol{B}$ and the majority (Δ_2) and minority (Δ_1) gap components. The last line shows the relative phase θ_{12} that specifies whether the superconducting ground state is s_{++} or $s_{\pm}$. In the vicinity of the impurity induced crossover line, the minority component of the order parameter is small, accounting for a few percent of the total density. The third column shows a vortex solution that features, in addition to the usual point singularities, a circular nodal line in the minority component Δ_1.

In order to investigate the properties of single-vortex solutions, the vector potential $\boldsymbol{A}$ and the gap functions $\Delta_{1,2}$ are discretized using a finite-element framework [19]. Starting with an initial configuration where both components have the same phase winding (i.e., at large distances $\Delta_i \propto e^{i\theta}$ where θ is the polar angle relative to the vortex center), the Ginzburg-Landau free energy (4) is then minimized using a nonlinear conjugate gradient algorithm. We begin by simulating the vortex solutions in zero external field. For that purpose, the vortices are induced only by the initial configuration of the phase winding. For further details on the numerical methods employed here, see for example the related discussion in [20].

Figure 2 shows the numerically calculated (isolated) vortex solutions in the vicinity of the impurity-induced crossover, in the case of a two-band superconductor with nearly degenerate bands and weak repulsive interband pairing interaction. Deep in the s_{++} and $s_{\pm}$ regimes (in the first and fourth column), the vortices have multicore structure where both components exhibit a vortex profile with different sizes of conventional cores, determined by the fundamental length scales. The vortex profiles of the minority component Δ_1 become very different when approaching the crossover line. On the $s_{\pm}$ side of the crossover, the minority component exhibits a strong overshoot near the core. The density overshoot effect, although much

smaller, was also reported in the microscopic model with one clean and one dirty band [21].

The very unconventional feature of vortices in this model of dirty two-band superconductors is the appearance of an additional circular nodal line of the minority component in addition to the usual point singularity at the center of the vortex [5]. While the bulk relative phase is zero (the s_{++} state) far from the vortex center, due to the competition between gradient and potential terms, it is more favorable to achieve a $\theta_{12} = \pi$ relative phase ($s_{\pm}$ state) in the vicinity of the core singularity. The transition between the "core" states with $\theta_{12} = \pi$ and the asymptotic state $\theta_{12} = 0$ is realized by nullifying the minority component at a given distance of the core, when the potential terms dominate over the gradient term. This can be seen in the third column of Fig. 2. Analytical explanation of such behavior was given in the previous work Ref. [5]. The existence of the circular nodal line results in the formation of a peculiar "moat"-like profile in the subdominant component of the superconducting gap. Note that the total superconducting order parameter does not vanish there; rather it is only the subdominant gap (here Δ_1) that vanishes exactly at this nodal line. Indeed, since it separates regions with $\theta_{12} = \pi$ from regions with zero phase difference, it has to be exactly zero somewhere. This can be viewed as a real-space counterpart of the crossover on the phase diagram. Namely, the line of direct crossover that separates the s_{++} state from the $s_{\pm}$ phase is that where the subdominant gap vanishes.

In order to understand how generic are such solutions, we further investigate numerically their existence on various phase diagrams. We find that the existence of these kinds of "moat-core" vortices does not depend on the specific values of the pairing coefficients. By that statement we mean that for the various different coupling matrices $\hat{\lambda}$ we investigated, we have been able to identify regions of the (T,Γ) diagram where "moat-core" vortices do form. This can be heuristically addressed with the following criterion that the condition for the transition of the vortex core structure is that the mixed-gradient energy (4b) dominates the Josephson energy (4c). This was discussed analytically in Ref. [5]. The investigation of the vortex solutions, for various parameter sets, rather shows that the moat-core is a common feature in the vicinity of the crossover line. The region of their existence is shown in Fig. 3. It is is clearly visible that the region with moat-core vortex solutions shrinks close to T_c and is eventually suppressed [panel (a) and (b)]. This is to be expected because near critical temperature, the solutions are dominated by a critical mode (see corresponding analytical estimates in [5]). For the investigated regimes, the width (in terms of impurities $\delta\Gamma$) of the regions where moat-core vortices exist increases with increasing the band disparity λ_{ii} [compare for example panels (b) and (d)]. By comparing panels (a), (b), and (c), it can also be seen that the width of the moat "region" increases with the interband coupling λ_{12}.

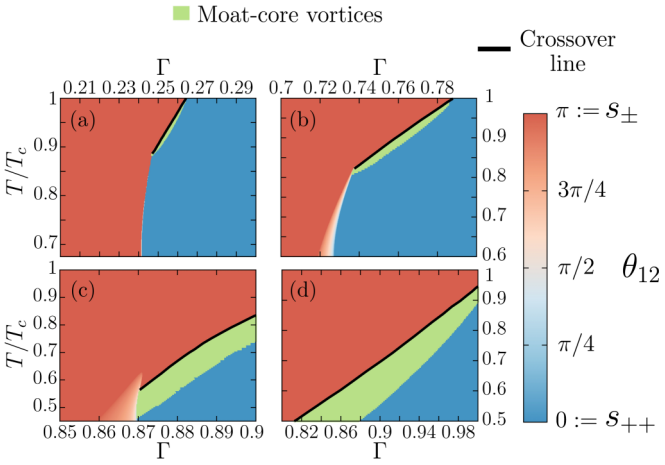

FIG. 3. Phase diagrams of the Ginzburg-Landau free energy (4) describing two-band superconductors with interband impurity scattering. These show the values of the lowest-energy state relative phase $\theta_{12} = \theta_2 - \theta_1$ between the components of the order parameter, and the regions of existence of moat-core vortices, as functions of the temperature and interband scattering Γ. In addition to the ground state properties, these diagrams shows the domains of existence of (isolated) moat-core vortices that feature a nodal line singularity surrounding the point singularity of the core. The different panels correspond to different values of the coupling matrix $\hat{\lambda}$. Panels (a), (b), and (c) respectively correspond to nearly degenerate bands with $\lambda_{11} = 0.29$ and $\lambda_{22} = 0.3$ with weak $\lambda_{12} = \lambda_{21} = -0.01$, intermediate $\lambda_{12} = \lambda_{21} = -0.05$, and strong $\lambda_{12} = \lambda_{21} = -0.1$ repulsive interband pairing interaction. The last panel (d) describes the case of intermediate band disparity $\lambda_{11} = 0.25$ and $\lambda_{22} = 0.3$ with intermediate $\lambda_{12} = \lambda_{21} = -0.05$ repulsive interband pairing interaction. The solid black line shows the zero of Δ_2, which is the crossover between $s_{\pm}$ and s_{++} states. It is clear here that (isolated) vortices with nodal zero line are quite generic solutions in the vicinity of the crossover line.

IV. PHASE COEXISTENCE IN EXTERNAL FIELD AND MAGNETIC-FIELD-DRIVEN CROSSOVER

In this section, we consider the effect in the presence of intervortex interactions and its implication for states of dirty two-band superconductors in an external magnetic field. First of all the existence of these moat-core vortices, where both $s_{\pm}$ and s_{++} phases coexist, implies that a lattice of such vortices would represent a special kind of phase coexistence and that, in an external field, the sharp crossover found in the ground state is rather washed out to a finite region in the parameter space.

In order to investigate the response to an applied external magnetic field $\boldsymbol{H} = H_z \boldsymbol{e}_z$, perpendicular to the plane, the Gibbs free energy $\mathcal{G} = \mathcal{F} - \boldsymbol{B} \cdot \boldsymbol{H}$ is minimized, with requiring that $\nabla \times \boldsymbol{A} = \boldsymbol{B}_{ext}$ on the boundary (for details, see a related discussion in Ref. [20]).

Figure 4 demonstrates the external-magnetic-field-driven crossover between the $s_{\pm}$ and s_{++} states. The coupling parameters are those of Fig. 2, and the temperature and the strength of the interband impurity scattering place the system in the bulk s_{++} state, close to the crossover line. The computations are thus performed for parameters where the single-vortex solutions have a circular nodal line similar to that shown in the third column in Fig. 2. In zero and low external fields, the preferred phase locking in the bulk is $\theta_{12} = 0$ (the s_{++} state). Upon increasing the external field, vortices start to enter the domain, introducing small inclusions of state with $\theta_{12} = \pi$ in their core. When the density of vortices becomes significant, the

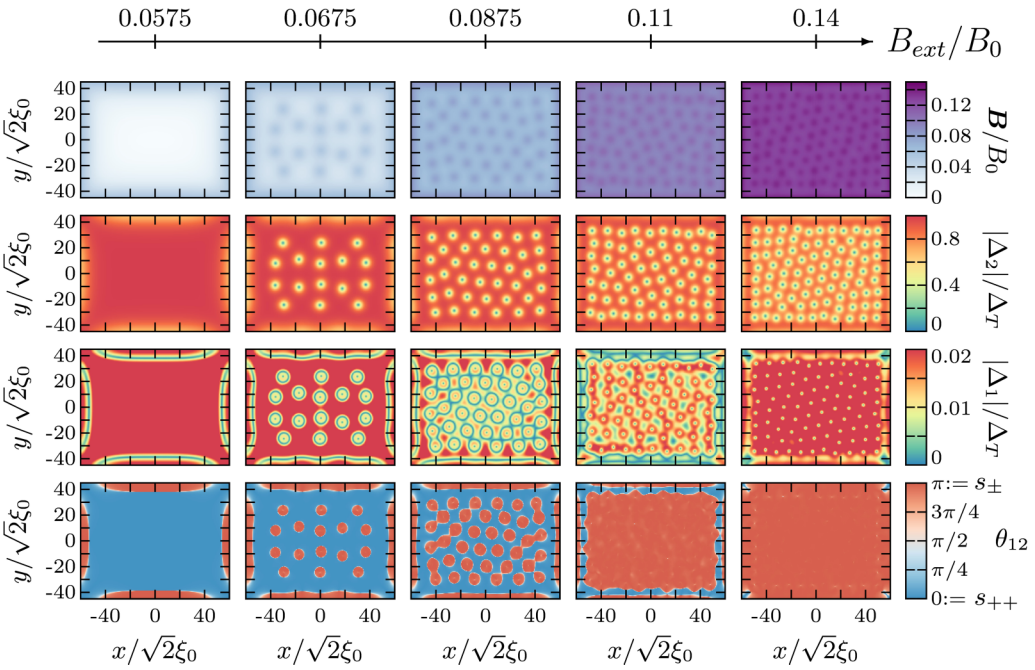

FIG. 4. Magnetization process of a dirty two-band superconductor. The coupling parameters are those of Fig. 2, the temperature is $T/T_c = 0.9$, $q = 0.5$, and the strength of the interband impurity scattering $\Gamma = 0.7625$ places the system in the bulk s_{++} state, in the vicinity of the crossover line. That choice of parameters gives single-vortex solutions with the circular nodal line similar to that of the third column in Fig. 2. The different lines respectively display the magnetic field $\boldsymbol{B}$ and the majority (Δ_2) and minority (Δ_1) gap components. The last line shows the relative phase θ_{12} that specifies whether the superconducting ground state is s_{++} or $s_{\pm}$. The preferred phase locking in the bulk is $\theta_{12} = 0$ (the s_{++} state). Upon increasing external field, vortices start to enter the system, introducing small blobs of $\theta_{12} = \pi$ in their moat core. When the density of vortices becomes significant, the cores of the subdominant component start to overlap. As can be seen in the third column, at intermediate vortex densities there appear regions where blobs of the $\theta_{12} = \pi$ phase merge. When the field is increased further the whole system shows a $\theta_{12} = \pi$ phase locking everywhere. Note that on the last line the system has the s_{++} state in the bulk but $s_{\pm}$ state near the boundary. By contrast at elevated fields the system becomes an $s_{\pm}$ superconductor in the bulk, while a layer of s_{++} forms close to a boundary.

cores of the subdominant component start to overlap until the whole system shows the $\theta_{12} = \pi$ phase locking everywhere. Thus the crossover here is driven by the external magnetic field.

We find that even in a low applied field, below the first critical field, the Meissner state also exhibits the unusual property of coexistence of both s_{++} and $s_{\pm}$ states. Indeed, the $s_{\pm}$ state can be realized near the boundaries while in the bulk, it is the s_{++} state. That is, as can be seen from the first column of Fig. 4, the region carrying Meissner currents shows a $\theta_{12} = \pi$ phase locking (thus an $s_{\pm}$ state near boundaries), while the bulk is in the s_{++} state (with $\theta_{12} = 0$). This current-carrying region with $\theta_{12} = \pi$ is separated from the $\theta_{12} = 0$ bulk by a nodal line of the subdominant component. That nodal line originates in the competition between phase-locking kinetic terms favoring a $\theta_{12} = \pi$ relative phase in the current-carrying regions, and potential terms that favor zero phase difference. The reversal of the phase locking in the current-carrying region is thus in some sense similar to that occurring in vortex cores in the vicinity of the crossover [5].

As illustrated in Fig. 4, the magnetization properties in the vicinity of the $s_{\pm}/s_{++}$ crossover are rather unusual. It is also interesting to consider the case of a field-cooled simulation close to the impurity-induced crossover. Figure 5 displays a simulation of a field-cooled experiment at a constant applied field that starts at temperatures placing the system above the crossover line in the $s_{\pm}$ phase, and that ends in the s_{++} phase. This field-cooled path is denoted by the vertical line displayed in the phase diagram of Fig. 1. Sufficiently far from the crossover, the relative phase corresponds to that of the bulk properties in zero field, i.e., the $s_{\pm}$ phase for temperatures above the crossover line and s_{++} below the crossover. However, unlike the zero-field case, there is no sharp crossover between both states. As can be seen in the third column, after the crossover, the vortex-carrying regions remain mostly with the $s_{\pm}$ phase because the cores of the subdominant component still overlap. When going away from the crossover, that is, when further decreasing the temperature, the cores in the subdominant component Δ_1 do not overlap anymore. Still the vortices with zero nodal line feature inclusion of the $\theta_{12} = \pi$ state while the intervortex spaces have relative phase $\theta_{12} = 0$. That situation of a lattice (or liquid) of moat-core vortices thus represents a phase coexistence or a mircoemulsion of $s_{\pm}$ inclusions inside the s_{++} state.

V. CONCLUSION

We considered a two-band superconducting system that has an impurity-driven $s_{\pm}/s_{++}$ crossover line. We generalize

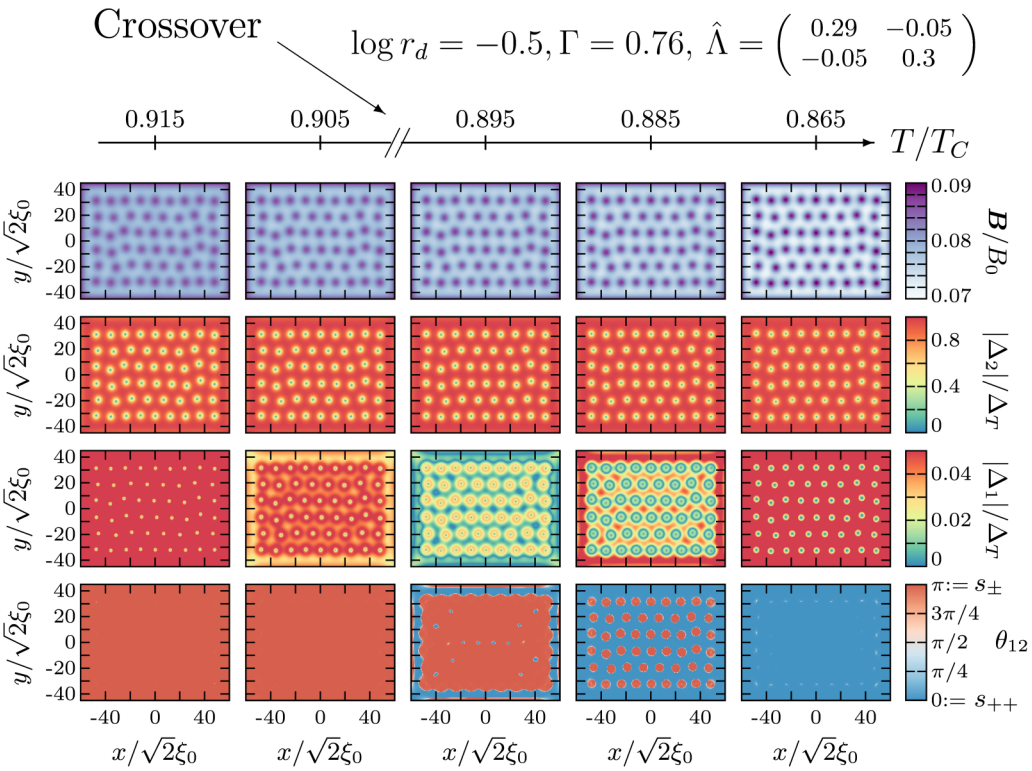

FIG. 5. A field-cooled state simulation for a dirty two-band superconductor, in the vicinity of the impurity induced crossover line. The displayed quantities are the same as in Fig. 4. The preferred phase locking at high temperatures is $\theta_{12} = \pi$ (the $s_\pm$ state), while it is $\theta_{12} = 0$ (the s_{++} state) at low temperatures. Decreasing the temperatures drives the system across the crossover line. After the crossover, vortices still carry inclusions of $\theta_{12} = \pi$ in their core. Only far below the crossover temperature, vortices do not carry different phase locking in their core anymore, and the whole system shows a $\theta_{12} = 0$ phase locking everywhere.

the zero-field phase diagram to the case where the system is subjected to external magnetic field. We report that it is a rather generic feature that on the s_{++} side of this crossover, the vortex solutions are unconventional, featuring a circular nodal line that segregates the $s_\pm$ phase inclusions in the cores from the bulk s_{++} phase. Further, we demonstrated that as a consequence of such vortex solutions, the behavior of dirty two-band superconductors in the vicinity of the crossover is also rich in an external field. Indeed, in contrast to the zero-field picture of a sharp crossover, the lattice and liquids of moat-core vortices represent a lattice or a "mircoemulsion" of $s_\pm$ inclusions inside the s_{++} state. Moreover, as the vortex density raises in increasing field, there is also a field-induced crossover from s_{++} to the $s_\pm$, which can be resolved in local phase-sensitive probes [22–24]. We also pointed out that in these systems in an applied external field, the superconducting state near the Meissner current carrying boundary can be $s_\pm$ while it is s_{++} in the bulk. This result has direct implications for local probes of superconducting states, such as the one proposed in Refs. [22–24], and for Josephson junction experiments. The coexistence state will manifest itself in the existence of signatures of both the $s_\pm$ and s_{++} states depending on the probe's position. The formation of nodal lines was also found in a different phenomenological clean three-band model where it arises for a different reason due to frustrated Josephson terms [13] rather than originating from competition between mixed-gradient and potential terms. That suggests that the phenomenon is rather generic and applies also to other models featuring a crossover from the $s_\pm$ to s_{++} state.

ACKNOWLEDGMENTS

The work was supported by Swedish Research Council Grants No. 642-2013-7837 and No. VR2016-06122 and the Goran Gustafsson Foundation for Research in Natural Sciences and Medicine. M.S. was supported by the Academy of Finland (Project No. 297439). The computations were performed on resources provided by the Swedish National Infrastructure for Computing (SNIC) at National Supercomputer Center at Linköping, Sweden.

APPENDIX: GINZBURG-LANDAU COEFFICIENTS

Table I shows the actual values of the coefficients entering the Ginzburg-Landau functional that were used for the various simulations throughout the paper.

TABLE I. Coefficients of the Ginzburg-Landau free energy functional (4), which correspond to the various numerical simulations reported in the main body of the text. They are calculated using the formulas (5), (6), (7), and (8), derived consistently from the microscopic Usadel theory (1). The last column shows the effective Josephson coupling $J_{\rm eff} = 2(a_{12} + c_{11}|\Delta_1|^2 + c_{22}|\Delta_2|^2)$. Positive (resp. negative) values of $J_{\rm eff}$ denote the $s_{\pm}$ (resp. s_{++}) phase, while $J_{\rm eff} = 0$ exactly at the crossover.

	Control parameter	$k_{11} = k_{22}$ ($\times 10^{-1}$)	k_{12} ($\times 10^{-1}$)	a_{11} ($\times 10^{-2}$)	a_{22} ($\times 10^{-2}$)	a_{12} ($\times 10^{-3}$)	$b_{11} = b_{22}$ ($\times 10^{-1}$)	b_{12} ($\times 10^{-3}$)	$c_{11} = c_{22}$ ($\times 10^{-2}$)	c_{12} ($\times 10^{-3}$)	$J_{\rm eff}$ ($\times 10^{-2}$)
	$\Gamma = 0.253$	4.57854	0.373521	3.46285	–2.29089	–0.1615	0.741321	–2.80412	0.329015	0.3137	0.17184
	$\Gamma = 0.256$	4.58081	0.37838	3.46165	–2.29209	–0.86902	0.742242	–2.83503	0.333393	0.321875	0.03220
Fig. 2	$\Gamma = 0.257$	4.58157	0.380002	3.46123	–2.29251	–1.10501	0.742549	–2.84532	0.334855	0.324627	–0.01427
	$\Gamma = 0.260$	4.58386	0.384875	3.45997	–2.29377	–1.81332	0.743474	–2.87614	0.339251	0.332965	–0.15349
Fig. 4	$\boldsymbol{B}/B_0$	4.45512	1.06235	8.70857	2.95483	–106.676	0.721483	–4.72472	0.884065	2.48617	–19.6283
	$T/T_c = 0.915$	8.94251	3.90581	3.40222	–2.51494	–4.11727	2.89522	–3.8533	6.31571	32.5610	0.29833
	$T/T_c = 0.905$	9.02277	3.96752	3.06348	–2.85368	–6.22441	2.94601	–3.44763	6.47026	33.5801	0.00939
Fig. 5	$T/T_c = 0.895$	9.10466	4.03077	2.72175	–3.19541	–8.36281	2.99822	–3.01249	6.63016	34.6403	–0.28168
	$T/T_c = 0.885$	9.18824	4.09562	2.37699	–3.54017	–10.5332	3.05192	–2.54593	6.79565	35.7439	–0.57084
	$T/T_c = 0.865$	9.36067	4.23033	1.67808	–4.23908	–14.9731	3.16401	–1.51015	7.14448	38.0905	–1.12672

[1] I. I. Mazin, D. J. Singh, M. D. Johannes, and M. H. Du, Unconventional Superconductivity with a Sign Reversal in the Order Parameter of $LaFeAsO_{1-x}F_x$, Phys. Rev. Lett. **101**, 057003 (2008).

[2] A. V. Chubukov, D. V. Efremov, and I. Eremin, Magnetism, superconductivity, and pairing symmetry in iron-based superconductors, Phys. Rev. B **78**, 134512 (2008).

[3] P. J. Hirschfeld, M. M. Korshunov, and I. I. Mazin, Gap symmetry and structure of Fe-based superconductors, Rep. Prog. Phys. **74**, 124508 (2011).

[4] D. V. Efremov, M. M. Korshunov, O. V. Dolgov, A. A. Golubov, and P. J. Hirschfeld, Disorder-induced transition between $s_{\pm}$ and s_{++} states in two-band superconductors, Phys. Rev. B **84**, 180512 (2011).

[5] J. Garaud, M. Silaev, and E. Babaev, Change of the vortex core structure in two-band superconductors at the impurity-scattering-driven $s_{\pm}/s_{++}$ crossover, Phys. Rev. B **96**, 140503 (2017).

[6] A. Gurevich, Enhancement of the upper critical field by nonmagnetic impurities in dirty two-gap superconductors, Phys. Rev. B **67**, 184515 (2003).

[7] For the question of formal validity of the multiband expansion see the discussion of the clean case [8].

[8] M. Silaev and E. Babaev, Microscopic derivation of two-component Ginzburg-Landau model and conditions of its applicability in two-band systems, Phys. Rev. B **85**, 134514 (2012).

[9] M. Silaev, J. Garaud, and E. Babaev, Phase diagram of dirty two-band superconductors and observability of impurity-induced $s + is$ state, Phys. Rev. B **95**, 024517 (2017).

[10] A. M. Bobkov and I. V. Bobkova, Time-reversal symmetry breaking state near the surface of an $s_{\pm}$ superconductor, Phys. Rev. B **84**, 134527 (2011).

[11] T. K. Ng and N. Nagaosa, Broken time-reversal symmetry in Josephson junction involving two-band superconductors, Europhys. Lett. **87**, 17003 (2009).

[12] V. Stanev and Z. Tešanović, Three-band superconductivity and the order parameter that breaks time-reversal symmetry, Phys. Rev. B **81**, 134522 (2010).

[13] J. Carlström, J. Garaud, and E. Babaev, Length scales, collective modes, and type-1.5 regimes in three-band superconductors, Phys. Rev. B **84**, 134518 (2011).

[14] S. Maiti and A. V. Chubukov, $s + is$ state with broken time-reversal symmetry in Fe-based superconductors, Phys. Rev. B **87**, 144511 (2013).

[15] V. Stanev and A. E. Koshelev, Complex state induced by impurities in multiband superconductors, Phys. Rev. B **89**, 100505 (2014).

[16] J. Böker, P. A. Volkov, K. B. Efetov, and I. Eremin, $s + is$ superconductivity with incipient bands: Doping dependence and STM signatures, Phys. Rev. B **96**, 014517 (2017).

[17] V. Grinenko, P. Materne, R. Sarkar, H. Luetkens, K. Kihou, C. H. Lee, S. Akhmadaliev, D. V. Efremov, S.-L. Drechsler, and H.-H. Klauss, Superconductivity with broken time-reversal symmetry in ion-irradiated $Ba_{0.27}K_{0.73}Fe_2As_2$ single crystals, Phys. Rev. B **95**, 214511 (2017).

[18] J. Garaud, A. Corticelli, M. Silaev, and E. Babaev, Properties of dirty two-bands superconductors with repulsive interband interaction: normal modes, length scales, vortices and magnetic response, arXiv:1802.07252 [cond-mat.supr-con].

[19] F. Hecht, New development in Freefem++, J. Numer. Math. **20**, 251 (2012).

[20] J. Garaud, E. Babaev, T. A. Bojesen, and A. Sudbø, Lattices of double-quanta vortices and chirality inversion in $p_x + ip_y$ superconductors, Phys. Rev. B **94**, 104509 (2016).

[21] K. Tanaka, M. Eschrig, and D. F. Agterberg, Theory of vortices in hybridized ballistic/diffusive-band superconductors, Phys. Rev. B **75**, 214512 (2007).

[22] P. J. Hirschfeld, D. Altenfeld, I. Eremin, and I. I. Mazin, Robust determination of the superconducting gap sign structure via quasiparticle interference, Phys. Rev. B **92**, 184513 (2015).

[23] Z. Du, X. Yang, D. Altenfeld, Q. Gu, H. Yang, I. Eremin, P. J. Hirschfeld, I. I. Mazin, H. Lin, X. Zhu, and H.-H. Wen, Sign reversal of the order parameter in $(Li_{1-x}Fe_x)OHFe_{1-y}Zn_ySe$, Nat. Phys. **14**, 134 (2017).

[24] D. Altenfeld, P. J. Hirschfeld, I. I. Mazin, and I. Eremin, Detecting sign-changing superconducting gap in LiFeAs using quasiparticle interference, arXiv:1712.03625.